are two possible orientations for this group, with refined group occupancies of 54.8 (5)% for the "B" form and 45.2 (5)% for the "A" form.

An absorption correction was applied.[25] Final refinement was carried out with anisotropic thermal parameters for all non-hydrogen atoms that were not disordered. Hydrogen atoms were included at calculated positions with use of a riding model except for those bonded to the disordered ethyl carbons. Isotropic thermal parameters for the hydrogen atoms were fixed at 1.2 times that of the bonded carbon. The largest peak in a final difference map had a value of 0.69 e $Å^{-3}$ and is located near the disordered ethyl peroxide.

Acknowledgment. We thank the National Institutes of Health (GM 26226) for financial support.

Supplementary Material Available: Table of atomic coordinates, bond lengths, bond angles, hydrogen atom positions, and anisotropic thermal parameters for $TPPGe(OCH_2CH_3)_2$ and $TPPGe(OOCH_2CH_3)_2$ (18 pages); tables of observed and calculated structure factors for these two complexes (46 pages). Ordering information is given on any current masthead page.

Synthetic Design of a Multielectron Series of Homologous Dirhodium Fluorophosphines Possessing an Emissive $d\sigma^*$ Excited State

Joel I. Dulebohn, Donald L. Ward, and Daniel G. Nocera*,†

Contribution from the Department of Chemistry and the LASER Laboratory, Michigan State University, East Lansing, Michigan 48824. *Received August 3, 1989*

Abstract: A novel homologous series of $Rh_2(0,0)$, $Rh_2(0,II)$, and $Rh_2(II,II)$ bis(difluorophosphino)methylamine complexes have been synthesized and structurally and electronically characterized. These binuclear rhodium compounds are all prepared from the reaction of $[RhCl(PF_3)_2]_2$ with $CH_3N(PF_2)_2$. Under reducing conditions, $Rh_2[CH_3N(PF_2)_2]_3(PF_3)_2$ (**1**) is isolated in moderate yields. Orange crystals of **1**, prepared by layering hexane over a dichloromethane solution of **1**, are triclinic with a space group $P\bar{1}$, $a = 10.021$ (4) Å, $b = 10.139$ (4) Å, $c = 14.299$ (7) Å, $\alpha = 74.95$ (3)°, $\beta = 76.79$ (3)°, $\gamma = 62.17$ (3)°, $V = 1230.9$ (9) $Å^3$, and $Z = 2$. The structure was refined to $R = 0.067$ and $R_w = 0.078$. Conversely, reaction of $[RhCl(PF_3)_2]_2$ with $CH_3N(PF_2)_2$ in the presence of the oxidant $Cl_2IC_6H_5$ produces $Rh_2[CH_3N(PF_2)_2]_3Cl_4$ (**3**) in high yields. Yellow needles of **3**, obtained from an ether–THF solution, are monoclinic with a space group $C2/c$; the cell parameters are $a = 15.462$ (2) Å, $b = 10.999$ (2) Å, $c = 14.256$ (2) Å, $\beta = 107.52$ (1)°, $V = 2312.0$ (6) $Å^3$, and $Z = 4$. Compound **3** contains a crystallographic C_2 axis. After refinement $R = 0.042$ and $R_w = 0.045$. In the absence of oxidants and reductants, the unsymmetrical mixed-valence $Rh_2[CH_3N(PF_2)_2]_3Cl_2(PF_3)$ (**2**) complex is obtained. The molecular structure of **2** is a composite of **1** and **3** in that the trigonal-bipyramidal coordination geometry about Rh(0) centers in **1** and the octahedral coordination at the Rh(II) centers in **3** are retained about the mixed-valence $Rh_2(0,II)$ core. For each complex the ligands are rotated considerably from an eclipsed conformation. The Rh···Rh separations of 2.841 (2), 2.785 (1), and 2.707 (1) Å in **1**, **2**, and **3**, respectively, are consistent with the presence of a Rh–Rh single bond. Electronic structural considerations suggest that the metal–metal bond results from the overlap of the one-electron-occupied d_{z^2} orbitals of rhodium centers. Accordingly, **1**, **2**, and **3** comprise an electronically related series best represented as $(d^8)d^1$–$d^1(d^8)$, $(d^8)d^1$–$d^1(d^6)$, and $(d^6)d^1$–$d^1(d^6)$, respectively. Electronic absorption spectra are dominated by intense bands, which are characteristic of $\sigma \rightarrow d\sigma^*$ transitions. Crystalline solids of **1**, **2**, and **3** exhibit red, long-lived emissions ($\tau = 53$, 79, and 287 μs, respectively) upon excitation with frequencies coincident with the absorption manifold. Luminescence is consistent with a $d\sigma^*$ excited-state parentage of primarily triplet character.

Transition-metal complexes in electronic excited states can exhibit unique chemical reactivity. Whereas some excited-state processes follow dissociative reaction pathways, many transition-metal complexes exist as discrete molecular species in thermally equilibrated excited states,[1-4] For the latter case, the thermodynamic driving force for the reaction exceeds that of the ground state by an amount comparable to the internal energy of the excited state. This increased driving force is oftentimes manifested in the excited state overcoming large thermodynamic and/or kinetic barriers confronting the corresponding ground-state species. A central theme of inorganic photochemistry has been to exploit these thermodynamic and kinetic enhancements to promote novel oxidation–reduction reactions.[5-11] Because many important reactions involve multielectron transformations, recent attention has been focused on developing photochemical schemes in which the photoreagent effects a multielectron process. Although guidelines for multielectron photoreactivity have begun to emerge,[12-16] few photochemical schemes have been realized in which the initial multielectron photoreagent is regenerated.[17,18] As is the case for the photoreactant, the multielectron photoproduct typically resides in deep thermodynamic or kinetic wells that hinder its conversion back to the desired photoreactive state.

† Alfred P. Sloan Fellow and NSF Presidential Young Investigator.

(1) Juris, A.; Balzani, V.; Barigelletti, F.; Campagna, S.; Belser, P.; von Zelewsky, A. *Coord. Chem. Rev.* **1988**, *84*, 85-277.
(2) *Photochemistry and Photophysics of Coordination Compounds*; Yersin, H., Vogler, A., Eds.; Springer-Verlag: Berlin, 1987.
(3) Adamson, A. W. *J. Chem. Educ.* **1983**, *60*, 797-802.
(4) Porter, G. B. In *Concepts of Inorganic Photochemistry*; Adamson, A. W., Fleischauer, P. D., Eds.; Wiley: New York, 1975.
(5) *Photoinduced Electron Transfer*; Fox, M. A., Chanon, M., Eds.; Elsevier: Amsterdam, 1988; Part D.
(6) Meyer, T. J. *Acc. Chem. Res.* **1989**, *22*, 163-170.
(7) Kavarnos, G. J.; Turro, N. J. *Chem. Rev.* **1986**, *86*, 401-449.
(8) Balzani, V.; Sabbatini, N.; Scandola, F. *Chem. Rev.* **1986**, *86*, 319-337.
(9) *Energy Resources through Photochemistry and Catalysis*; Grätzel, M., Ed.; Academic Press: New York, 1983.
(10) Gray, H. B.; Maverick, A. W. *Science* **1981**, *214*, 1201-1205.
(11) *Photochemical Conversion and Storage of Solar Energy*; Connolly, J. S., Ed.; Academic Press: New York, 1981.
(12) (a) Roundhill, D. M.; Gray, H. B.; Che, C.-M. *Acc. Chem. Res.* **1989**, *22*, 55-61. (b) Marshall, J. L.; Steigman, A. E.; Gray, H. B. In *Excited States and Reactive Intermediates*; Lever, A. B. P., Ed.; ACS Symposium Series 307; American Chemical Society: Washington, DC, 1986; pp 166-176 and references therein. (c) Caspar, J. V.; Gray, H. B. *J. Am. Chem. Soc.* **1984**, *106*, 3029-3030.

0002-7863/90/1512-2969$02.50/0

It is not unreasonable to expect, therefore, that these kinetic or thermodynamic barriers of the photoproduct, in principle, can be surmounted by channeling the regenerative reaction via the excited state of the photoproduct. In this manner, photocatalytic schemes can be constructed. The success of this approach necessarily relies on the design of a series of multielectron reagents, each of which possesses a long-lived excited state.

To this end, we became interested in the possibility of synthesizing a homologous series of excited-state complexes, which are interrelated by multielectron steps. Our strategy has depended primarily on the ability to employ a ligating coordination sphere capable of stabilizing metal redox centers in a variety of formal oxidation states while engendering electronic structural properties that are compatible with a rich excited-state redox chemistry. For these reasons, we turned our attention to the chemistry of fluorophosphine metal complexes. The good π-accepting and moderate σ-donating[19-24] ability of bidentate fluorophosphine ligands is manifested in their ability to stabilize metal centers in low and high oxidation states, respectively.[25] Specifically, we were intrigued with the bidentate bis(difluorophosphino)alkyl/arylamines, $RN(PF_2)_2$ (R = methyl, phenyl), owing to the elegant studies of King and co-workers,[26] which establish the precedence for this ligand to give rise to a diverse redox chemistry of bimetallic cores. The unique redox properties of metals coordinated by this ligand are best exemplified by the cobalt complex $Co_2[CH_3N(PF_2)_2]_3(CO)_2$, which upon treatment with Br_2 gives the $Co_2(II,II)$ derivative $Co_2[CH_3N(PF_2)_2]_3(CO)_2Br_4$[27] and upon its electrochemical reduction yields the $Co_2(-I,-I)$ anion $Co_2[CH_3N(PF_2)_2]_3(CO)_2^{2-}$.[28] In this system, the bis(difluorophosphino)methylamine ligand has stabilized the metal core to an overall six-electron change in formal oxidation state! Moreover, the cobalt complex emphasizes the ability of the $RN(PF_2)_2$ ligand to coordinate across singly bonded metal–metal (M–M) cores. Recent work by us[29] and Miskowski et al,[30] has demonstrated intense luminescence from M–M $d\sigma^*$ excited states. Not unexpectedly, the $d\sigma^*$ excited state is highly distorted and consequently the presence of a bidentate ligand possessing a single bridgehead atom can greatly enhance the $d\sigma^*$ emission intensity and lifetime by circumventing nonradiative decay pathways arising from metal–metal dissociation. Indeed, the dual function of the $RN(PF_2)_2$ ligand to stabilize different oxidation states and to give rise to attractive excited-state properties is illustrated by our recent preparation of the unsymmetrical complex $Rh_2[CH_3N(PF_2)_2]_3Cl_2(PF_3)$,[29] in which $d\sigma^*$ luminescence is observed from a metal core comprised of rhodium in two different oxidation states, Rh(0) and Rh(II). The existence of this compound suggested to us that the corresponding $Rh_2(0,0)$ and $Rh_2(II,II)$ complexes could be prepared, and electronic structural considerations led us to believe that the $d\sigma^*$ excited state would be preserved. We now report the synthesis and structural and spectroscopic characterization of a homologous $Rh_2(0,0)$, $Rh_2(0,II)$, and $Rh_2(II,II)$ bis(difluorophosphino)methylamine series. Interestingly, long-lived luminescence characteristic of a $d\sigma^*$ excited state is observed for each of these novel binuclear complexes. The series provides an interesting example of how a discrete excited state can be synthetically incorporated among a series of multielectron congeners.

Experimental Section

General Procedures. Syntheses of the binuclear rhodium complexes, unless otherwise stated, were performed under argon atmospheres by using standard Schlenk-line techniques. The starting compounds $[RhCl(PF_3)_2]_2$ and $CH_3N(PF_2)_2$ and the oxidant (dichloroiodo)benzene ($Cl_2IC_6H_5$) were prepared by literature methods.[31-33] All solvents were deoxygenated, dried, and freshly distilled prior to use. Cobaltocene (Strem Chemical Co.) and phosphorus trifluoride (Ozark-Mahoning Co.) were used as received.

Synthesis of Dirhodium Complexes. $Rh_2[CH_3N(PF_2)_2]_3(PF_3)_2$ (1). In a typical reaction, 0.58 mL of $CH_3N(PF_2)_2$ (0.83 g, 5.0 mmol) was delivered by syringe to a dichloromethane solution containing 0.701 g (1.12 mmol) of $[RhCl(PF_3)_2]_2$. The change in solution color from orange to red was accompanied by the liberation of PF_3. Upon cessation of the gas evolution, the solution was charged with 0.422 g (2.23 mmol) of $Co(C_5H_5)_2$ from a sidearm. The mixture was stirred for 10 min under PF_3, and the cobaltocenium that had formed was removed by filtration. Addition of 10 mL of hexane led to further precipitation of cobaltocenium and excess cobaltocene. Filtration under argon yielded a red solution that was vacuum distilled to dryness to produce 0.691 g of an orange-brown precipitate. The solid was introduced onto a Florisil column and eluted with a hexane–dichloromethane (85:15%) solution. The fraction was distilled to dryness under vacuum to give an orange-yellow precipitate. Yield 0.311 g (0.352 mmol), 32%. Orange crystals of **1**, suitable for X-ray diffraction studies, were obtained from dichloromethane solutions layered with hexane.

$Rh_2[CH_3N(PF_2)_2]_3Cl_2(PF_3)$ (2). To a solution of 0.300 g (0.477 mmol) of $[RhCl(PF_3)_2]_2$ in 15 mL of benzene was added 0.24 g (1.4 mmol) of $CH_3N(PF_2)_2$. The yellow solution turned red and PF_3 gas was liberated. After stirring for 20 min, the solution was filtered, and the volume of the filtrate was reduced to approximately 10 mL. Addition of 15 mL of hexane led to the precipitation of an orange solid, which was collected by filtration under an argon flow, washed with benzene, and dried in vacuo. Yield 0.102 g (0.118 mmol), 25%. Red-orange crystals of **2** were obtained by layering a CH_2Cl_2 solution of the complex with hexane under argon.

$Rh_2[CH_3N(PF_2)_2]_3Cl_4$ (3). $[RhCl(PF_3)_2]_2$ (0.397 g, 0.627 mmol) was dissolved in 15 mL of benzene. The solution turned dark red immediately upon the addition of 0.44 mL (3.8 mmol) of $CH_3N(PF_2)_2$ and then lightened within seconds. After a few minutes of stirring, $Cl_2IC_6H_5$ (0.700 g, 2.55 mmol) was added, prompting the solution to turn yellow. The suspension was refluxed for 4 h, and a yellow precipitate was filtered off under argon, washed with benzene, and dried under vacuum. Yield 0.315 g (0.371 mmol), 59%. X-ray-quality yellow crystals of **3** were prepared by diffusing ether into a THF solution of the complex under argon.

Spectroscopic Measurements. Electronic absorption spectra were recorded on dichloromethane solutions (HPLC grade) of the binuclear rhodium complexes with a Cary 17 spectrophotometer. Extinction coefficients, which were determined by use of high-vacuum cells consisting of a 1-cm quartz cuvette and a 10-mL sidearm, were calculated from Beer–Lambert plots composed of at least five points. Time-resolved and steady-state luminescence spectra were recorded on previously described Nd:YAG pulsed laser (λ_{exc} = 355 nm, fwhm = 8 ns) and high-resolution emission instruments (λ_{exc} = 365 nm), respectively.[34,35] All

(13) (a) Rodman, G. S.; Daws, C. A.; Mann, K. R. *Inorg. Chem.* **1988**, *27*, 3347–3353. (b) Rodman, G. S.; Mann, K. R. *Inorg. Chem.* **1985**, *24*, 3507–3508.
(14) (a) Hill, C. L.; Bouchard, D. A.; Kadkhodayan, M.; Williamson, M. M.; Schmidt, J. A.; Hilinski, E. F. *J. Am. Chem. Soc.* **1988**, *110*, 5471–5479. (b) Hill, C. L.; Bouchard, D. A. *J. Am. Chem. Soc.* **1985**, *107*, 5148–5157.
(15) Chang, I.-J.; Nocera, D. G. *J. Am. Chem. Soc.* **1987**, *109*, 4901–4907.
(16) Caspar, J. V. *J. Am. Chem. Soc.* **1985**, *107*, 6718–6719.
(17) Che, C.-M.; Lee, W.-M.; Cho, K.-C. *J. Am. Chem. Soc.* **1988**, *110*, 5407–5411.
(18) Harvey, E. L.; Stiegman, A. E.; Vlcek, A., Jr.; Gray, H. B. *J. Am. Chem. Soc.* **1987**, *109*, 5233–5235.
(19) Orpen, A. G.; Connelly, N. G. *J. Chem. Soc., Chem. Commun.* **1985**, 1310–1311.
(20) Marynick, D. S. *J. Am. Chem. Soc.* **1984**, *106*, 4064–4065.
(21) Xiao, S.-X.; Trogler, W. C.; Ellis, D. E.; Berkovitch-Yellin, Z. *J. Am. Chem. Soc.* **1983**, *105*, 7033–7037.
(22) Avanzino, S. C.; Chen, H.-W.; Donahue, C. J.; Jolly, W. L. *Inorg. Chem.* **1980**, *19*, 2201–2205.
(23) Corderman, R. R.; Beauchamp, J. L. *Inorg. Chem.* **1978**, *17*, 1585–1588.
(24) Savariault, J.-M.; Serafini, A.; Pelissier, M.; Cassoux, P. *Theor. Chim. Acta* **1976**, *42*, 155–161.
(25) Nixon, J. F. *Adv. Inorg. Chem. Radiochem.* **1985**, *29*, 41–141.
(26) King, R. B. *Acc. Chem. Res.* **1980**, *13*, 243–248.
(27) Newton, M. G.; Pantaleo, N. S.; King, R. B.; Lotz, T. J. *J. Chem. Soc., Chem. Commun.* **1978**, 514–515.
(28) Chaloyard, A.; El Murr, N.; King, R. B. *J. Organomet. Chem.* **1980**, *188*, C13–C15.
(29) Dulebohn, J. I.; Ward, D. L.; Nocera, D. G. *J. Am. Chem. Soc.* **1988**, *110*, 4054–4056.
(30) (a) Stiegman, A. E.; Miskowski, V. M. *J. Am. Chem. Soc.* **1988**, *110*, 4053–4054. (b) Stiegman, A. E.; Miskowski, V. M.; Gray, H. B. *J. Am. Chem. Soc.* **1986**, *108*, 2781–2782.
(31) Bennett, M. A.; Patmore, D. J. *Inorg. Chem.* **1971**, *10*, 2387–2395.
(32) Nixon, J. F. *J. Chem. Soc. A* **1968**, 2689–2692.
(33) Lucas, H. J.; Kennedy, E. R. In *Organic Syntheses*; Horning, E. C., Ed.; Wiley: New York, 1955; Vol. 3, pp 482–483.
(34) Newsham, M. D.; Giannelis, E. P.; Pinnavaia, T. J.; Nocera, D. G. *J. Am. Chem. Soc.* **1988**, *110*, 3885–3891.
(35) Mussell, R. D.; Nocera, D. G. *J. Am. Chem. Soc.* **1988**, *110*, 2764–2772.

Table I. Crystal Data for **1**, **2**, and **3**

	1	**2**	**3**
formula	$Rh_2F_{18}P_8N_3C_3H_9$	$Rh_2F_{15}Cl_2P_7N_3C_3H_9$	$Rh_2F_{12}Cl_4P_6N_3C_3H_9$
formula wt	882.70	865.64	848.57
cryst dimens, mm	0.14 × 0.32 × 0.44	0.36 × 0.45 × 0.56	0.04 × 0.10 × 0.42
cryst system	triclinic	orthorhombic	monoclinic
space group	$P\bar{1}$	$P2_12_12_1$	$C2/c$
unit cell parameters			
a, Å	10.021 (4)	9.620 (2)	15.462 (2)
b, Å	10.139 (4)	12.755 (2)	10.999 (2)
c, Å	14.299 (7)	19.564 (3)	14.256 (2)
α, deg	74.95 (3)	90	90
β, deg	76.79 (3)	90	107.52 (1)
γ, deg	62.17 (3)	90	90
V, Å^3	1230.9 (9)	2400.6 (6)	2312.0 (6)
Z	2	4	4
ρ_{calcd}, g/cm^3	2.38	2.40	2.44
μ(Mo Kα), cm^{-1}	19.7	21.5	23.8
radiation (λ, Å)	Mo Kα (0.71073)	Mo Kα (0.71073)	Mo Kα (0.71073)
temp, °C	23 (1)	27 (1)	−70 (3)
orientation reflctns no., range	25, 15 < 2θ < 24	15, 20 < 2θ < 25	23, 15 < 2θ < 20
scan method	θ–2θ	θ–2θ	θ–2θ
scan rate, deg min^{-1}	4	4	4
data col range, 2θ, deg	4.5 < 2θ < 50	4.5 < 2θ < 65	4.5 < 2θ < 45
no. of unique data, total with $F_o^2 > 3\sigma(F_o^2)$	4172, 3149	4889, 3880	2560, 1623
no. of parameters refined	307	290	137
trans factors, min, max	0.759, 1.363	0.465, 0.547	0.789, 1.153
R^a	0.067	0.026	0.042
$R_w{}^b$	0.078	0.025	0.045
GOF^c	3.14	1.20	2.54
largest shift/esd, final cycle	0.11	0.15	0.14
largest peak, e/Å^3	1.01 (18)	0.57 (7)	0.68 (8)

$^a R = \sum||F_o| - |F_c||/\sum|F_o|$. $^b R_w = [\sum w(|F_o| - |F_c|)^2/\sum w|F_o|^2]^{1/2}$; $w = 1/\sigma^2(|F_o|)$. ^{c}Goodness of fit = $[\sum w(|F_o| - |F_c|)^2/(N_{obsd} - N_{parameters})]^{1/2}$.

Table II. Atomic Positional and Isotropic Displacement (Å^2) Parameters for $Rh_2[CH_3N(PF_2)_2]_3(PF_3)_2$ (**1**)^a

atom	x	y	z	B/Å^2
Rh(1)	0.1433 (1)	0.7525 (1)	0.72377 (8)	4.19 (3)
Rh(2)	0.2718 (1)	0.9001 (1)	0.79385 (8)	4.12 (3)
P(1)	0.2870 (5)	0.7771 (5)	0.5849 (3)	6.4 (1)
P(2)	0.4753 (4)	0.7929 (5)	0.6908 (3)	5.5 (1)
P(3)	−0.0786 (4)	0.9434 (5)	0.7599 (3)	5.1 (1)
P(4)	0.0807 (5)	1.1139 (4)	0.7367 (3)	5.0 (1)
P(5)	0.2357 (4)	0.5608 (4)	0.8454 (3)	5.1 (1)
P(6)	0.2353 (4)	0.7682 (4)	0.9400 (3)	4.9 (1)
P(7)	0.0472 (5)	0.6428 (5)	0.6695 (4)	6.9 (1)
P(8)	0.3708 (5)	1.0138 (5)	0.8463 (4)	6.6 (1)
F(1)	0.334 (1)	0.665 (1)	0.5174 (8)	10.9 (4)
F(2)	0.223 (1)	0.923 (1)	0.5013 (8)	11.1 (5)
F(3)	0.581 (1)	0.875 (1)	0.6520 (9)	9.1 (3)
F(4)	0.605 (1)	0.628 (1)	0.7260 (9)	9.1 (4)
F(5)	−0.214 (1)	0.978 (1)	0.7059 (8)	8.3 (3)
F(6)	−0.170 (1)	0.937 (1)	0.8620 (7)	7.9 (3)
F(7)	0.030 (1)	1.2552 (9)	0.7847 (8)	8.2 (3)
F(8)	0.098 (1)	1.199 (1)	0.6290 (7)	7.7 (3)
F(9)	0.150 (1)	0.463 (1)	0.8860 (8)	8.3 (3)
F(10)	0.392 (1)	0.425 (1)	0.8320 (8)	8.4 (4)
F(11)	0.351 (1)	0.726 (1)	1.0128 (7)	8.5 (3)
F(12)	0.092 (1)	0.838 (1)	1.0133 (7)	8.5 (4)
F(13)	0.147 (1)	0.478 (1)	0.6463 (9)	11.1 (4)
F(14)	−0.0807 (9)	0.608 (1)	0.7324 (9)	8.9 (3)
F(15)	−0.028 (1)	0.716 (1)	0.5756 (8)	13.2 (4)
F(16)	0.411 (1)	1.136 (1)	0.7778 (9)	9.8 (4)
F(17)	0.524 (1)	0.921 (1)	0.884 (1)	11.4 (4)
F(18)	0.278 (1)	1.107 (1)	0.9268 (8)	9.6 (3)
N(1)	0.453 (1)	0.777 (1)	0.584 (1)	6.3 (4)
N(2)	−0.088 (1)	1.113 (1)	0.7419 (8)	5.3 (3)
N(3)	0.240 (1)	0.600 (1)	0.9514 (9)	5.4 (3)
C(1)	0.580 (2)	0.742 (2)	0.504 (1)	10.2 (7)
C(2)	−0.233 (2)	1.259 (2)	0.735 (1)	7.6 (5)
C(3)	0.257 (2)	0.489 (2)	1.045 (1)	8.6 (7)

^{a}Anisotropically refined atoms are given in the form of the isotropic equivalent displacement parameter defined as $^4/_3[a^2B_{11} + b^2B_{22} + c^2B_{33} + ab(\cos\gamma)B_{12} + ac(\cos\beta)B_{13} + bc(\cos\alpha)B_{23}]$.

Table III. Atomic Positional and Isotropic Displacement (Å^2) Parameters for $Rh_2[CH_3N(PF_2)_2]_3Cl_2(PF_3)$ (**2**)^a

atom	x	y	z	B/Å^2
Rh(1)	0.27066 (5)	0.00685 (4)	0.07903 (3)	3.020 (7)
Rh(2)	0.10328 (5)	0.07458 (4)	0.18646 (2)	2.934 (7)
Cl(1)	0.4119 (2)	−0.0632 (2)	−0.0133 (1)	5.75 (4)
Cl(2)	0.4552 (2)	0.1142 (2)	0.1206 (1)	4.36 (4)
P(1)	0.1040 (2)	−0.0907 (2)	0.0379 (1)	4.25 (4)
P(2)	−0.0719 (2)	−0.0123 (2)	0.14032 (9)	3.32 (3)
P(3)	0.3668 (2)	−0.1162 (2)	0.1473 (1)	4.61 (4)
P(4)	0.2632 (2)	0.0029 (2)	0.25600 (9)	4.17 (4)
P(5)	0.2086 (2)	0.1511 (2)	0.0202 (1)	3.98 (4)
P(6)	0.1393 (2)	0.2383 (1)	0.1468 (1)	3.41 (3)
P(7)	−0.0261 (3)	0.1256 (2)	0.2709 (1)	5.12 (5)
F(1)	0.0737 (6)	−0.0770 (5)	−0.0388 (2)	8.0 (1)
F(2)	0.1319 (6)	−0.2101 (4)	0.0360 (4)	7.9 (1)
F(3)	−0.2015 (5)	0.0526 (4)	0.1190 (3)	6.4 (1)
F(4)	−0.1563 (5)	−0.0903 (4)	0.1855 (3)	6.4 (1)
F(5)	0.3211 (7)	−0.2324 (4)	0.1391 (3)	7.4 (2)
F(6)	0.5224 (5)	−0.1346 (5)	0.1350 (4)	8.3 (2)
F(7)	0.2082 (6)	−0.0451 (4)	0.3241 (2)	6.4 (1)
F(8)	0.3748 (6)	0.0732 (5)	0.2911 (3)	7.0 (1)
F(9)	0.0881 (7)	0.1439 (5)	−0.0310 (3)	7.7 (1)
F(10)	0.3184 (7)	0.1906 (4)	−0.0307 (3)	7.0 (1)
F(11)	0.0138 (5)	0.3143 (4)	0.1539 (3)	5.5 (1)
F(12)	0.2456 (5)	0.3147 (3)	0.1805 (3)	5.4 (1)
F(13)	−0.1496 (8)	0.1924 (7)	0.2555 (4)	14.7 (2)
F(14)	−0.0945 (7)	0.0494 (5)	0.3182 (3)	9.7 (2)
F(15)	0.0331 (9)	0.1919 (6)	0.3257 (3)	12.3 (2)
N(1)	−0.0524 (6)	−0.0831 (5)	0.0701 (3)	3.9 (1)
N(2)	0.3614 (7)	−0.0963 (6)	0.2291 (4)	5.2 (2)
N(3)	0.1749 (6)	0.2571 (5)	0.0646 (3)	3.8 (1)
C(1)	−0.1715 (8)	−0.1436 (7)	0.0391 (5)	5.8 (2)
C(2)	0.449 (1)	−0.159 (1)	0.2783 (6)	9.7 (3)
C(3)	0.186 (1)	0.3651 (6)	0.0349 (5)	5.6 (2)

^{a}Anisotropically refined atoms are given in the form of the isotropic equivalent displacement parameter defined as $^4/_3[a^2B_{11} + b^2B_{22} + c^2B_{33} + ab(\cos\gamma)B_{12} + ac(\cos\beta)B_{13} + bc(\cos\alpha)B_{23}]$.

luminescence spectra were corrected for the instrument response function. Variable-temperature luminescence and lifetime measurements were recorded on samples cooled with an Air Products closed-cycle cryogenic system by methods described elsewhere.[34]

X-ray Crystallography. The diffraction data for the dirhodium complexes were collected on a Nicolet P3/F diffractometer using graphite-monochromated Mo Kα (λ = 0.71073 Å) radiation. The intensity data

Table IV. Atomic Positional and Isotropic Displacement (Å²) Parameters for $Rh_2[CH_3N(PF_2)_2]_3Cl_4$ (3)[a]

atom	x	y	z	B/Å²
Rh(1)	0.03788 (4)	0.25217 (7)	0.17586 (4)	1.824 (9)
Cl(1)	0.0943 (1)	0.2502 (3)	0.0352 (1)	3.18 (4)
Cl(2)	0.1755 (1)	0.1618 (2)	0.2759 (2)	3.25 (5)
P(1)	−0.0044 (2)	0.0537 (5)	0.1500 (2)	2.61 (4)
P(3)	−0.0846 (2)	0.3444 (2)	0.0873 (2)	2.71 (4)
P(4)	−0.1147 (2)	0.4203 (2)	0.2637 (2)	3.01 (5)
F(1)	0.0586 (4)	−0.0229 (5)	0.1078 (3)	3.4 (1)
F(2)	−0.0952 (4)	0.0165 (5)	0.0756 (4)	3.7 (1)
F(5)	−0.0708 (4)	0.4334 (5)	0.0092 (4)	3.9 (1)
F(6)	−0.1588 (3)	0.2650 (6)	0.0166 (4)	4.2 (1)
F(7)	0.0747 (4)	0.5480 (5)	0.1973 (4)	4.5 (1)
F(8)	0.2071 (4)	0.4332 (6)	0.2189 (4)	4.8 (1)
N(1)	0.000	−0.0257 (9)	0.250	3.0 (2)
N(2)	−0.1389 (4)	0.4340 (7)	0.1439 (5)	2.7 (1)
C(1)	0.000	−0.163 (1)	0.250	6.3 (5)
C(2)	−0.2091 (6)	0.5243 (9)	0.0866 (8)	4.0 (2)

[a] Anisotropically refined atoms are given in the form of the isotropic equivalent displacement parameter defined as $^4/_3[a^2B_{11} + b^2B_{22} + c^2B_{33} + ab(\cos\gamma)B_{12} + ac(\cos\beta)B_{13} + bc(\cos\alpha)B_{23}]$.

were collected by using θ–2θ scans at a rate of 4°/min (in 2θ). See Table I for crystal parameters and details of intensity collection. All calculations were performed on a VAX 11/750 computer by using SDP/VAX.[36] Positional parameters for **1**–**3** are listed in Tables II–IV, respectively. Complete tables of bond distances, bond angles, anisotropic thermal parameters, hydrogen atom parameters, and structure factors are available as supplementary material.

$Rh_2[CH_3N(PF_2)_2]_3(PF_3)_2$. An orange irregularly shaped crystal of **1** (dimensions 0.14 × 0.32 × 0.44 mm) was mounted on a glass fiber. The cell parameters and orientation matrix were obtained from least-squares refinement of 25 reflections in the range $15 < 2\theta < 24°$. The space group was found to be $P\bar{1}$.

A total of 4552 reflections was collected, of which 4172 were unique and not systematically absent. Three standard reflections were measured every 93 reflections and indicated a decrease of intensity of 15.2%; a decay correction was applied.

The structure was solved by Patterson heavy-atom methods. The coordination sphere was completed by an alternating series of least-squares cycles and difference Fourier syntheses. The hydrogen atoms were placed in idealized positions and constrained to ride on the carbon atoms. Anisotropic refinements were used to give $R = 0.067$ and $R_w = 0.078$. The largest shift-to-error was 0.11σ, and the largest peak in the final difference map was 1.01 (18) e/Å³.

$Rh_2[CH_3N(PF_2)_2]_3Cl_2(PF_3)$. An irregular-shaped red-orange crystal of **2** (dimensions 0.36 × 0.45 × 0.56 mm) was mounted in a glass capillary in a random orientation. The cell constants and an orientation matrix were obtained from least-squares refinement of 15 reflections in the range $20 < 2\theta < 25°$. From systematic absences and from refinement, the space group was determined to be $P2_12_12_1$.

A total of 9542 reflections was collected, of which 4889 were unique and not systematically absent. Corrections were applied and the structure was solved as described for **1**. The non-hydrogen atoms were refined with anisotropic thermal parameters, and hydrogen atoms were placed in idealized positions and constrained to ride on the carbon atoms. The largest shift-to-error was 0.15σ, and the largest peak in the final difference map was 0.57 (7) e/Å³. The structural results for the solution of **2** have previously been reported.[29]

$Rh_2[CH_3N(PF_2)_2]_3Cl_4$. A yellow transparent needle of **3** (crystal dimensions 0.04 × 0.10 × 0.42 mm) was mounted with Paratone-N oil and cooled with a nitrogen gas stream to −70 °C. The cell constants and an orientation matrix were obtained from least-squares refinement of 23 reflections in the range $15 < 2\theta < 20°$. From the systematic absences and from refinement, the space group was determined to be $C2/c$.

A total of 2957 reflections was collected. Corrections were applied and the structure was solved as described for **1**. The non-hydrogen atoms were refined with anisotropic thermal parameters, and hydrogen atoms were placed in idealized positions and constrained to ride on the carbon atoms. Atoms N(1) and C(1) lie along a crystallographic twofold axis that passes midway between the two rhodium atoms; only half of the atoms are crystallographically unique. The largest shift-to-error was 0.14σ, and the largest peak in the final difference map was 0.68 (8) e/Å³.

(36) Frenz, B. A. In *Computing in Crystallography*; Schenk, H., Olthof-Hazelkamp, R., Vankonigsveld, H., Bassi, G. C., Eds; Delft University Press: Delft, Holland, 1978; pp 64–71.

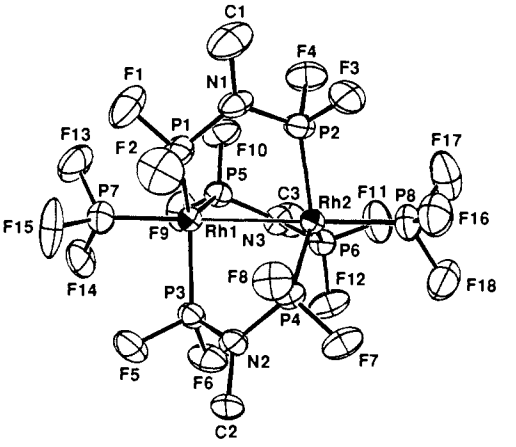

Figure 1. ORTEP drawing and numbering scheme of $Rh_2[CH_3N(PF_2)_2]_3(PF_3)_2$ (**1**) with 30% probability thermal ellipsoids. For clarity hydrogen atoms are not shown. Selected bond distances and angles are listed in Table V.

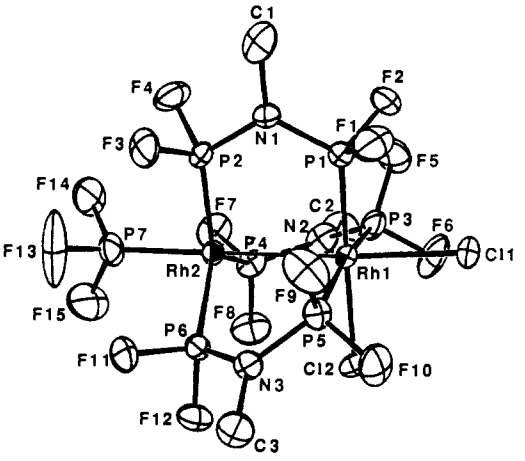

Figure 2. ORTEP view of $Rh_2[CH_3N(PF_2)_2]_3Cl_2(PF_3)$ (**2**) showing the numbering scheme. Thermal parameters are shown at the 50% level. Hydrogen atoms are omitted for the sake of clarity. Table VI lists selected bond distances and angles.

Results

Synthesis of Dirhodium Complexes. The $[RhCl(PF_3)_2]_2$ dimer reacts smoothly with bis(difluorophosphino)methylamine to yield **2**, and under reducing the oxidizing conditions to yield **1** and **3**, respectively. The formation of **2** corresponds to an intramolecular disproportionation of the $Rh_2(I,I)$ starting material. However, the intimate mechanism, the nature of which is still under investigation, appears to be more complicated owing to our isolation and characterization from reaction mixtures of the recently reported trimer $Rh_3(\mu\text{-}Cl)_3(\mu\text{-}CH_3N(PF_2)_2)_3$.[37] We have observed that reaction of this trimetallic complex with excess ligand leads to **2** in good yields.

The unsymmetrical binuclear complex can be viewed as a synthon for **1** and **3**. The former is derived from the reduction of the Rh(0) center of **2** with subsequent trappng by PF_3, whereas **3** can be envisaged to form from the oxidation of the Rh(0) center by chlorine. Indeed, although **1** and **3** are prepared from the aforementioned $[RhCl(PF_3)_2]_2$ starting compound in high yields, we have been able to directly convert among **1**, **2**, and **3** with the appropriate choice of oxidizing and reducing conditions. For instance, oxidation of **1** by $Cl_2IC_6H_5$ readily affords **3**. Conversely, sodium borohydride reduction of **3** produces **1**, but admittedly in low yields. As expected, both **1** and **3** can directly be obtained from **2**. The ability to synthetically interconvert among these Rh_2 complexes underscores the fluorophosphine ligand's capacity to

(37) Mague, J. T.; Johnson, M. P.; Lloyd, C. L. *J. Am. Chem. Soc.* **1989**, *111*, 5012–5013.

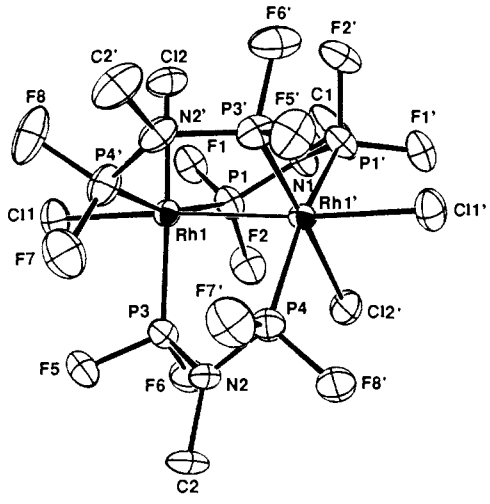

Figure 3. Perspective ORTEP view and labeling scheme of $Rh_2[CH_3N(PF_2)_2]_3Cl_4$ (**3**). The thermal ellipsoids are at the 50% probability level; hydrogens are not shown. Selected bond distances and bond angles are listed in Table VII.

Table V. Selected Bond Distances (Å) and Bond Angles (Deg) for $Rh_2[CH_3N(PF_2)_2]_3(PF_3)_2$ (**1**)[a]

Bond Distances			
Rh(1)-Rh(2)	2.841 (2)	Rh(2)-P(2)	2.214 (4)
Rh(1)-P(1)	2.203 (4)	Rh(2)-P(4)	2.225 (3)
Rh(1)-P(3)	2.222 (3)	Rh(2)-P(6)	2.224 (4)
Rh(1)-P(5)	2.227 (4)	Rh(2)-P(8)	2.176 (6)
Rh(1)-P(7)	2.134 (7)		

Bond Angles			
Rh(2)-Rh(1)-P(1)	86.0 (2)	Rh(1)-Rh(2)-P(2)	85.2 (2)
Rh(2)-Rh(1)-P(3)	85.4 (2)	Rh(1)-Rh(2)-P(4)	85.4 (2)
Rh(2)-Rh(1)-P(5)	86.4 (2)	Rh(1)-Rh(2)-P(6)	86.0 (2)
Rh(2)-Rh(1)-P(7)	179.4 (1)	Rh(1)-Rh(2)-P(8)	179.5 (1)
P(1)-Rh(1)-P(3)	120.6 (2)	P(2)-Rh(2)-P(4)	118.6 (2)
P(1)-Rh(1)-P(5)	121.2 (1)	P(2)-Rh(2)-P(6)	119.7 (1)
P(1)-Rh(1)-P(7)	93.4 (2)	P(2)-Rh(2)-P(8)	94.5 (2)
P(3)-Rh(1)-P(5)	116.8 (1)	P(4)-Rh(2)-P(6)	119.9 (1)
P(3)-Rh(1)-P(7)	94.7 (2)	P(4)-Rh(2)-P(8)	94.5 (2)
P(5)-Rh(1)-P(7)	94.1 (2)	P(6)-Rh(2)-P(8)	94.5 (2)

Torsional Bond Angles	
P(1)-Rh(1)-Rh(2)-P(2)	-30.39 (17)
P(3)-Rh(1)-Rh(2)-P(4)	-32.29 (16)
P(5)-Rh(1)-Rh(2)-P(6)	-29.07 (16)

[a] Bond distance and angle numbers in parentheses are estimated standard deviations in the least significant digits.

readily accommodate metal cores in a variety of formal oxidation states.

Structural Interpretation. The molecular structures adopted by **1–3** are unique for dirhodium chemistry; they are represented by the ORTEP diagrams reproduced in Figures 1–3. For the purposes of comparison, the previously reported ORTEP diagram of **2**[29] has been included. The presence of three bidentate fluorophosphine ligands in these structures is unusual and in contrast to the trans coordination of two bidentate ligands of the ubiquitous A-frame structures for dirhodium complexes.[38-40] Complexes **1–3** are structurally distinguished among themselves by their rhodium coordination environments, of which there are two basic types. As illustrated by the inner coordination spheres depicted in Figure 4, trigonal-bypyramidal and octahedral coordination gives rise to the symmetrical structures of **1** and **3**, respectively, and to the unsymmetrical structure of **2**. In the case of **1**, the

Table VI. Selected Bond Distances (Å) and Bond Angles (Deg) for $Rh_2[CH_3N(PF_2)_2]_3Cl_2(PF_3)$ (**2**)[a]

Bond Distances			
Rh(1)-Rh(2)	2.785 (1)	Rh(1)-P(5)	2.251 (2)
Rh(1)-Cl(1)	2.431 (2)	Rh(2)-P(2)	2.209 (2)
Rh(1)-Cl(2)	2.385 (2)	Rh(2)-P(4)	2.248 (2)
Rh(1)-P(1)	2.183 (2)	Rh(2)-P(6)	2.254 (2)
Rh(1)-P(3)	2.258 (2)	Rh(2)-P(7)	2.168 (2)

Bond Angles			
Rh(2)-Rh(1)-Cl(1)	176.46 (6)	P(1)-Rh(1)-P(5)	94.74 (8)
Rh(2)-Rh(1)-Cl(2)	89.69 (5)	P(3)-Rh(1)-P(5)	168.20 (8)
Rh(2)-Rh(1)-P(1)	91.73 (6)	Rh(1)-Rh(2)-P(2)	88.69 (5)
Rh(2)-Rh(1)-P(3)	90.36 (6)	Rh(1)-Rh(2)-P(4)	86.26 (5)
Rh(2)-Rh(1)-P(5)	88.79 (6)	Rh(1)-Rh(2)-P(6)	86.49 (5)
Cl(1)-Rh(1)-Cl(2)	92.81 (7)	Rh(1)-Rh(2)-P(7)	179.24 (7)
Cl(1)-Rh(1)-P(1)	85.81 (8)	P(2)-Rh(2)-P(4)	124.43 (8)
Cl(1)-Rh(1)-P(3)	87.43 (8)	P(2)-Rh(2)-P(6)	116.19 (7)
Cl(1)-Rh(1)-P(5)	93.94 (8)	P(2)-Rh(2)-P(7)	91.38 (8)
Cl(2)-Rh(1)-P(1)	178.32 (8)	P(4)-Rh(2)-P(6)	118.65 (8)
Cl(2)-Rh(1)-P(3)	83.83 (8)	P(4)-Rh(2)-P(7)	93.08 (8)
Cl(2)-Rh(1)-P(5)	84.40 (8)	P(6)-Rh(2)-P(7)	94.16 (8)
P(1)-Rh(1)-P(3)	97.05 (8)		

Torsional Bond Angles	
P(1)-Rh(1)-Rh(2)-P(2)	-4.81 (8)
P(3)-Rh(1)-Rh(2)-P(4)	22.76 (8)
P(5)-Rh(1)-Rh(2)-P(6)	-26.43 (7)

[a] Bond distance and angle numbers in parentheses are estimated standard deviations in the least significant digits.

Table VII. Selected Bond Distances (Å) and Bond Angles (Deg) for $Rh_2[CH_3N(PF_2)_2]_3Cl_4$ (**3**)[a,b]

Bond Distances			
Rh(1)-Rh(1)′	2.707 (1)	Rh(1)-P(1)	2.277 (2)
Rh(1)-Cl(1)	2.416 (2)	Rh(1)-P(4)′	2.226 (2)
Rh(1)-Cl(2)	2.392 (2)	Rh(1)-P(3)	2.184 (2)

Bond Angles			
Rh(1)′-Rh(1)-Cl(1)	175.75 (5)	Cl(1)-Rh(1)-P(4)′	92.56 (6)
Rh(1)′-Rh(1)-Cl(2)	92.94 (6)	Cl(2)-Rh(1)-P(1)	81.86 (8)
Rh(1)′-Rh(1)-P(1)	87.48 (7)	Cl(2)-Rh(1)-P(3)	176.86 (9)
Rh(1)′-Rh(1)-P(3)	87.01 (7)	Cl(2)-Rh(1)-P(4)′	80.75 (6)
Rh(1)′-Rh(1)-P(4)′	90.21 (2)	P(1)-Rh(1)-P(3)	101.28 (9)
Cl(1)-Rh(1)-Cl(2)	90.69 (8)	P(1)-Rh(1)-P(4)′	162.31 (6)
Cl(1)-Rh(1)-P(1)	90.85 (9)	P(3)-Rh(1)-P(4)′	96.11 (7)
Cl(1)-Rh(1)-P(3)	89.49 (9)		

Torsional Bond Angles	
P(1)-Rh(1)-Rh(1)′-P(1)′	32.61
P(3)-Rh(1)-Rh(1)′-P(4)	-28.43

[a] Atoms designated by the prime symbol are at $-x, +y, -^1/_2z$. [b] Bond distance and angle numbers in parentheses are estimated standard deviations in the least significant digits.

coordination geometry about each Rh(0) is nearly an ideal trigonal bipyramid whose equatorial plane is comprised of three phosphorus atoms from each of the bridging fluorophosphine ligands and whose apices are capped by the phosphorus of a terminal trifluorophosphine and by the neighboring Rh(0) of the binuclear core. The trigonal-bipyramidal coordination of the Rh(0) centers is contrasted by the pseudooctahedral ligation sphere of Rh(II). In **3**, the three phosphorus atoms of the individual fluorophosphine ligands adopt a meridional arrangement with a chlorine atom occupying the fourth site in the equatorial coordination plane. The pseudooctahedron about the Rh(II) is completed with the axial coordination of a chlorine atom and a Rh(II). The mutually trans arrangement of chlorines on adjacent Rh(II) centers has previously been postulated to be present in *trans*-$Rh_2Cl_2(CO)_2(dmpm)_2$ (dmpm = (dimethylphosphino)methane) and indeed observed for its chlorine oxidation product, *trans*-$Rh_2Cl_4(CO)_2(dmpm)_2$.[41] With **1** and **3** as structural benchmarks, we see that the unsymmetrical congener, **2**, is simply a structural composite of the $Rh_2(0,0)$ and $Rh_2(II,II)$ complexes in which the trigonal-bipy-

(38) Chaudret, B.; Delavaux, B.; Poilblanc, R. *Coord. Chem. Rev.* **1988**, *86*, 191–243.
(39) (a) Sutherland, B. R.; Cowie, M. *Inorg. Chem.* **1984**, *23*, 1290–1297. (b) Cowie, M.; Dwight, S. K. *Inorg. Chem.* **1979**, *18*, 2700–2706.
(40) Kubiak, C. P.; Eisenberg, R. *J. Am. Chem. Soc.* **1980**, *102*, 3637–3639.
(41) Jenkins, J. A.; Ennett, J. P.; Cowie, M. *Organometallics* **1988**, *7*, 1845–1853.

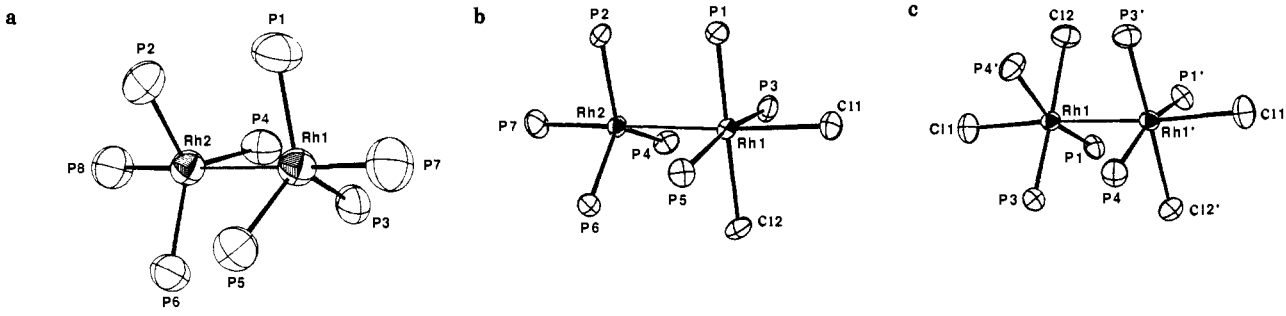

Figure 4. Skeletal view of the inner coordination spheres of (a) **1**, (b) **2**, and (c) **3**.

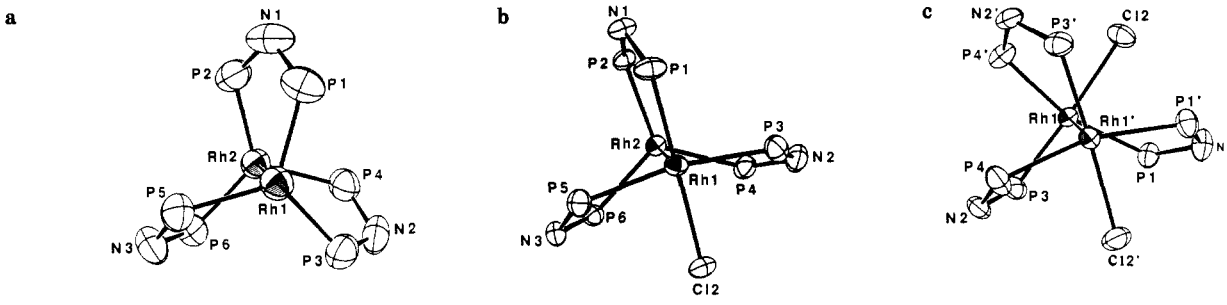

Figure 5. Structural framework of (a) **1**, (b) **2**, and (c) **3** as viewed nearly along the Rh–Rh axis. Axial ligands are omitted.

ramidal coordination about Rh(0) and octahedral coordination about Rh(II) are preserved.

Inspection of the selected bond angles and distances of **1–3** listed in Tables V–VII reveals several interesting trends. It is noteworthy that the Rh–Cl bonds trans to the rhodium–rhodium axis in **2** (d(Rh–Cl_{ax}) = 2.431 ± 0.002 Å) and **3** (d(Rh–Cl_{ax}) = 2.416 ± 0.002 Å) are significantly longer than the Rh–Cl bonds cis to it (d(Rh–Cl_{eq}) = 2.385 ± 0.002 Å in **2** and d(Rh–Cl_{eq}) = 2.392 ± 0.002 Å in **3**). Long axial Rh–Cl bonds have previously been attributed to the trans influence of the metal–metal bond.[42,43] However, in the case of **2** and **3**, it is not that the Rh–Cl_{ax} bonds are unusually long but rather that the Rh–Cl_{eq} bonds are short. These observations are congruent with simple bonding considerations. The good π-accepting ability of the fluorophosphine ligands should selectively enhance π donation from trans chlorine atoms. Accordingly, the π back-bonding between the rhodium and chlorine will be strengthened, thereby resulting in a shortening of the Rh–Cl_{eq} bond. This simple bonding model is further supported by comparison of Rh–P distances. The resulting synergism established between the π-donating chlorine and the π-accepting fluorophosphine not only should strengthen the Rh–Cl_{eq} bond but should also be manifested in increased π-back-bonding interactions between rhodium and the phosphorus trans to chlorine. This appears to be the case. As observed in Tables VI and VII, the Rh–P distances for phosphorus trans to chlorine (d(Rh–$P_{t,Cl}$) = 2.183 ± 0.002 Å in **2**, d(Rh–$P_{t,Cl}$) = 2.184 ± 0.002 Å in **3**) are at least 0.07 Å shorter than those for phosphorus trans to another phosphorus (d(Rh–$P_{t,P}$)$_{av}$ = 2.255 ± 0.002 Å in **2**, d(Rh–$P_{t,P}$)$_{av}$ = 2.252 ± 0.025 Å in **3**). The latter distances are more typical of normal Rh(II)–P bonds.[41,44,45]

As a concluding issue, we consider the Rh–Rh bond distances. Separations of 2.841 (2), 2.785 (1), and 2.707 (1) Å in **1**, **2**, and **3**, respectively, are indicative of a normal Rh–Rh single bond. The decrease along the series $Rh_2(0,0) > Rh_2(0,II) > Rh_2(II,II)$ is expected in view of the larger atomic radii of Rh(0) as compared to Rh(II). Although the Rh–Rh distances are considerably longer than those observed for rhodium carboxylates,[46–48] they are typical of Rh–Rh cores ligated by bidentate phosphines containing one bridgehead atom.[41,49–51] The presence of a single bond in **1–3**

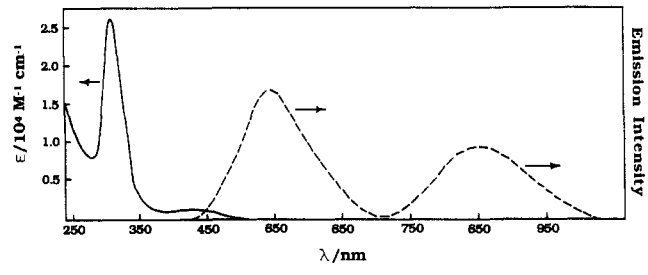

Figure 6. Electronic absorption spectrum (—) of **1** dissolved in CH_2Cl_2 at room temperature and corrected emission spectrum (---) of crystalline **1** at 77 K.

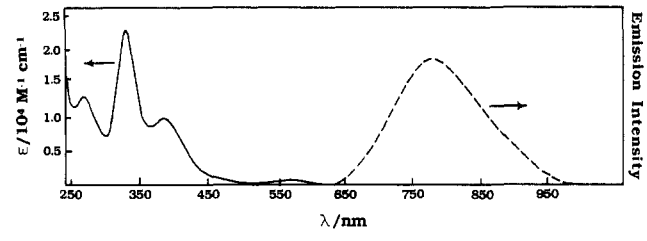

Figure 7. Electronic absorption spectrum (—) of **2** dissolved in CH_2Cl_2 at room temperature and corrected emission spectrum (---) of crystalline **2** at 77 K.

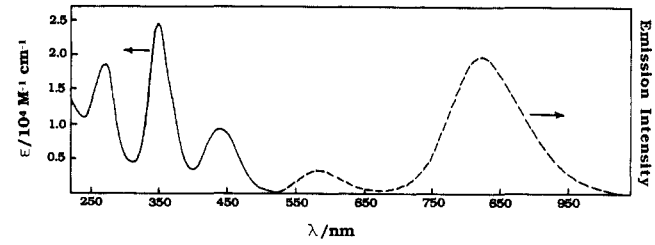

Figure 8. Electronic absorption spectrum (—) of **3** dissolved in CH_2Cl_2 at room temperature and corrected emission spectrum (---) of crystalline **3** at 77 K.

(42) (a) Gibson, J. A. E.; Cowie, M. *Organometallics* **1984**, *3*, 984–996. (b) Cowie, M.; Dwight, S. K. *Inorg. Chem.* **1980**, *19*, 209–216.
(43) Fair, J. P.; Olmstead, M. M.; Balch, A. L. *Inorg. Chem.* **1983**, *22*, 1229–1235 and references therein.
(44) Gibson, J. A. E.; Cowie, M. *Organometallics* **1984**, *3*, 722–731.
(45) Tortorelli, L. J.; Tucker, C. A.; Woods, C.; Bordner, J. *Inorg. Chem.* **1986**, *25*, 3534–3537.
(46) Boyar, E. R.; Robinson, S. D. *Coord. Chem. Rev.* **1983**, *50*, 109–208.
(47) Felthouse, T. R. *Prog. Inorg. Chem.* **1982**, *29*, 73–166.

Table VIII. Emission Spectral Data for Crystalline **1**, **2**, and **3** at 77 K

complex	λ_{max}, nm	τ, ns	λ_{max}, nm	τ, μs
1	540	<8	840	53
2[a]			780	79
3	580	<8	820	287

[a] No fluorescence is detected from solids of this compound.

induces significant rotation of the bridging fluorophosphine ligands away from an eclipsed conformation. The view along the nearly linear L–Rh–Rh–L′ (L, L′ = Cl or PF_3) bond axis of **1**–**3** (Figure 5) clearly reveals a twisted conformation of the bidentate ligands. Average torsional angles χ_{av} = 30.6° for **1** and χ_{av} = 30.5° for **3** are comparable to the 33.3° twist angle reported for the bis(difluorophosphino)methylamine ligands in $Co_2[CH_3N(PF_2)_2]_3(CO)_2$.[52] This remarkable flexibility of the bis(difluorophosphino)methylamine ligand allows the coordination asymmetry about the dirhodium core in **2** to be accommodated with facility and, indeed, undoubtedly plays a crucial role in the stabilization of the unusual mixed-valence Rh(0,II) species.

Electronic Absorption and Emission Spectra. The electronic absorption spectra of the dirhodium fluorophosphine complexes are shown in Figures 6–8. The spectra exhibit pronounced absorptions in the ultraviolet spectral region with less intense absorption bands in the visible. Red luminescence is observed from solids and low-temperature glasses of **1**–**3** upon excitation with frequencies coincident with the absorption manifold. In Figures 6–8 we show the emission spectra recorded on crystalline solids of **1**–**3** at 77 K. Each displays an intense band in the red spectral region, and **1** and **3** feature an additional emission to higher energy. The intensities of the emissions monotonically decrease with increasing temperature. Although luminescence from **3**, which is the brightest lumophore of the series, can be detected to room temperature, luminescence from **1** and **2** reaches the limits of our instrumentation by ~220 K. This temperature dependence in emission intensity is accompanied by an extreme temperature sensitivity of the full width at half-height of the emission band, increasing by approximately 1000–1500 cm^{-1} from 77 K to the highest temperatures at which emission can be detected. Emission spectra are vibrationally featureless and remain so to temperatures as low as 10 K. Luminescence was not detected from fluid solutions of any of the dirhodium complexes.

Insight into the nature of the luminescence comes from time-resolved spectroscopic measurements. The red emissions from **1**–**3** display similar behavior in that the lifetime decays are monoexponential and long. Microsecond lifetimes for **1**–**3** (Table VIII) are a signature of phosphorescence. Conversely, the decay of the higher energy emissions of **1** and **3** within the 8-ns temporal profile of the 355-nm excitation pulse from a Nd:YAG laser suggests to us that the red phosphorescence is accompanied by companion fluorescence. Interestingly, fluorescence from **2** could not be detected even at our instrument's highest sensitivity. In regard to the phosphorescence, the observed lifetime exhibits a pronounced temperature dependence of the form previously reported by us for **2**.[29] Namely, a low-temperature regime (10–60 K) in which the lifetime exhibits little variance is followed by a sharp monotonic decrease in lifetime with increasing temperature.

Discussion

Although cursory inspection of **1**–**3** suggests disparate molecular and electronic structures, closer examination shows these complexes to be quite similar. Trigonal-bipyramidal and octahedral coordination geometries, which are exclusively determined by the formal oxidation state of the rhodium metal centers, are preserved almost identically among the three complexes. Moreover, each of the binuclear complexes possesses a rhodium–rhodium single bond, and it is this bimetallic core and its associated axial ligands that appear to determine the electronic structure of this homologous series of complexes.

Absorption bands characteristic of the allowed transitions for M–M complexes dominate the electronic spectra of each of the dirhodium complexes. The absorption spectrum of **1**, typical of most single-bonded metal–metal dimers,[53,54] is dominated by an intense isolated band in the ultraviolet that is flanked by a broader less intense band to lower energy. The intensity, bandwidth, and position of the 305-nm band are signatures of a $\sigma \rightarrow d\sigma^*$ transition. The significant mixing of the metal–metal $d\sigma \rightarrow d\sigma^*$ transition with axial ligand-to-metal charge-transfer (LMCT) transitions, $L\sigma \rightarrow d\sigma^*$, which has previously been observed for a variety of metal complexes containing L–M–M–L (M = Rh, Ir, Pt; L = halide, SCN, OH) cores,[55] is not likely significant in **1** owing to the much higher lone-pair ionization potential of trifluorophosphine as compared to halides and pseudohalides. Consequently, the $\sigma \rightarrow d\sigma^*$ transition of **1** should be of relatively pure metal character. The lower energy, less intense absorption is analogous to the $d\pi^* \rightarrow d\sigma^*$ transitions of a variety of M–M complexes, including Pt_2(III,III) sulfates[54] and pyrophosphites,[55a,b] Rh_2(II,II) acetates and isocyanides,[55c] and dimanganese and dirhenium carbonyls.[56–58]

The absorption profiles of **2** and **3** are more complicated. Because the complexes are structurally unique, reliable assignment of the spectral features in Figures 7 and 8 is difficult without undertaking detailed spectroscopic measurements. Nevertheless, the spectra do display some useful qualitative information. Transitions arising from the ligand-based σ orbitals of the axial chloride ligands, in addition to the primarily metal-centered $\sigma \rightarrow d\sigma^*$ band, should be present. Inspection of Figures 7 and 8 indicates this to be the case; UV absorptions possessing band shapes and energies consistent with σ transitions are observed. The appearance of bands between 270 and 350 nm in the spectra of **2** and **3** is compatible with the location of ligand-based and configurationally mixed metal–ligand transitions of $Pt^{III,III}_2Cl_2$ and $Rh^{II,II}_2Cl_2$ complexes.[55] Moreover, the shift of $\sigma \rightarrow d\sigma^*$ transitions to lower energies with metal–ligand mixing has been observed to increase the absorptivity of the $d\pi^* \rightarrow d\sigma^*$ transition via intensity-stealing mechanisms.[55] The greater intensity of the absorption bands lying in the spectral region in which $d\pi^* \rightarrow d\sigma^*$ transitions typically occur (400–450 nm) for complexes **2** and **3** as compared to **1** is certainly consistent with the operation of similar $\sigma \rightarrow d\pi^*$ intensity-stealing mechanisms.

Our observation that electronic absorption is governed by the σ M–M framework of **1**–**3** is complemented by the luminescence properties of these complexes. The pronounced narrowing of the emission bands at lower temperatures is characteristic for luminescence of a state arising from excitation of an electron to a $d\sigma^*$ orbital.[30] Moreover, the invariance of the emission lifetime at low temperatures followed by a monotonic decrease with increasing temperature is a trend previously observed by us for the $d\sigma^*$ emission from $Pt^{III,III}_2L_2$ (L = Cl, Br, and H_2O) tetraphosphates.[59] Photophysical analysis of these Pt_2 complexes has

(48) Cotton, F. A.; Walton, R. A. *Multiple Bonds Between Metal Atoms*; Wiley-Interscience: New York, 1982, Chapter 7.
(49) (a) Cotton, F. A.; Eagle, C. T.; Price, A. C. *Inorg. Chem.* **1988**, *27*, 4362–4368. (b) Cotton, F. A.; Dunbar, K. R.; Verbruggen, M. G. *J. Am. Chem. Soc.* **1987**, *109*, 5498–5506.
(50) Balch, A. L.; Oram, D. E. *J. Organomet. Chem.* **1988**, *349*, 245–256.
(51) (a) Cowie, M.; Dickson, R. S. *Inorg. Chem.* **1981**, *20*, 2682–2688. (b) Cowie, M.; Dwight, S. K. *Inorg. Chem.* **1980**, *19*, 2508–2513. (c) Cowie, M. *Inorg. Chem.* **1979**, *18*, 286–292 and references therein.
(52) King, R. B.; Chang, M.; Newton, M. G. *J. Organomet. Chem.* **1985**, *296*, 15–30.
(53) Lever, A. B. P. *Inorganic Electronic Spectroscopy*; Elsevier: New York, 1984; Chapter 7.
(54) Miskowski, V. M.; Gray, H. B. In *Understanding Molecular Properties*; Avery, J., Dahl, J. P., Hansen, A. E., Eds.; Reidel: Dordrecht, Holland, 1987.
(55) (a) Che, C.-M.; Mak, T. C. W.; Miskowski, V. M.; Gray, H. B. *J. Am. Chem. Soc.* **1986**, *108*, 7840–7841. (b) Che, C.-M.; Butler, L. G.; Grunthaner, P. J.; Gray, H. B. *Inorg. Chem.* **1985**, *24*, 4662–4665. (c) Miskowski, V. M.; Smith, T. P.; Loehr, T. M.; Gray, H. B. *J. Am. Chem. Soc.* **1985**, *107*, 7925–7934.
(56) Harvey, P. D.; Butler, I. S.; de C. Barreto, M.; Coville, N. J.; Harris, G. W. *Inorg. Chem.* **1988**, *27*, 639–642.
(57) Jackson, R. A.; Poë, A. *Inorg. Chem.* **1978**, *17*, 997–1003.
(58) Wrighton, M. S.; Ginley, D. S. *J. Am. Chem. Soc.* **1975**, *97*, 2065–2072.

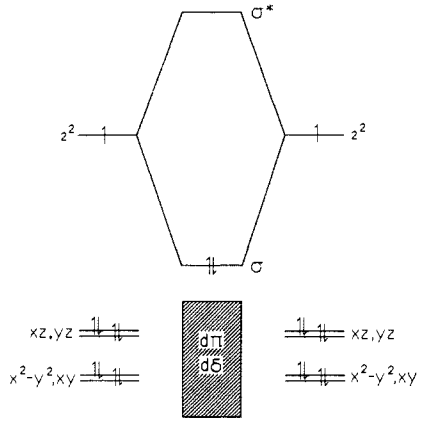

Figure 9. Simple molecular orbital diagram for the interaction of two C_{3v} Rh^0P_4 fragments. The dπ- and dσ-symmetry orbitals are filled and indicated by the shaded box. To minimize level congestion, the σ–σ* splitting is shown to be small and its manifold is isolated from that of the dπ and dδ orbitals.

revealed that the emissive excited state is the (B_{1u}, B_{2u}) spin–orbit component of the $^3(d\pi^* \rightarrow d\sigma^*)$ (i.e., ^3E_u) state. The temperature dependence arises from the thermal population of a higher energy deactivating state corresponding to the $E_u(^3E_u)$ spin–orbit component. We have since observed similar behavior for the observed lifetime of the $Pt^{III,III}_2L_2$ (L = Cl, Br, and I) pyrophosphites as well, and indeed, nonradiative deactivation by Boltzmann population within the $^3(d\pi^* \rightarrow d\sigma^*)$ spin–orbit manifold appears to be an emerging trend of dσ* luminescence for many M–M complexes. In the case of the dirhodium series, measured energy gaps of 1200 cm^{-1} conform well with those experimentally determined for the (B_{1u}, B_{2u})–E_u gap of $Pt^{III,III}_2L_2$ complexes and are in agreement with the 1000-cm^{-1} splittings predicted from first-order spin–orbit coupling calculations.[59] Finally, our observation that luminescence is not detected from solutions of **1–3** at temperatures equivalent to those at which the crystalline solids emit is consistent with recent photophysical studies and demonstrates the importance of medium rigidity as a crucial controlling factor of dσ* luminescence.[30]

Insight into the structural and spectroscopic properties of dirhodium complexes is provided by analysis of their electronic structure. We begin by considering the level structure of the C_{3v} Rh^0P_4 and C_{4v} $Rh^{II}P_3Cl_2$ fragments. Molecular orbital treatments[60,61] suggest that eight electrons of the d^9 Rh^0P_4 fragment reside in orbitals of $\pi(d_{xz}, d_{yz})$ and $\delta(d_{xy}, d_{x^2-y^2})$ symmetry, with the remaining electron occupying the $\sigma(d_{z^2})$ orbital. In the case of the d^7 $Rh^{II}P_3Cl_2$ fragment, the $d_{x^2-y^2}$ level is displaced to very high energies owing to the destabilizing σ* interactions of the metal with the ligands in the equatorial plane. Consequently, the odd electron of the d^7 $Rh^{II}P_3Cl_2$ fragment, as was the case for Rh^0P_4, resides in the $\sigma(d_{z^2})$ orbital, with the remaining six electrons residing in the lower energy $\pi(d_{xy}, d_{x^2-y^2})$ and $\delta(d_{xy})$ orbitals; low-symmetry splittings within the π orbitals have been ignored. Construction of the level diagrams for **1–3** is achieved by the orbital mixing of the appropriate rhodium fragments. These results are shown in Figures 9–11. The orbitals that will interact most strongly are those that extend perpendicularly from the equatorial plane of the fragments, namely, the spatially directed $\sigma(d_{z^2})$ orbitals. To a lesser extent the filled π-symmetry orbitals will interact, and negligible overlap will occur between the d orbitals, which are aligned parallel to each other. In each case, formation of a Rh–Rh single bond results from the pairing of the d_{z^2} electrons of the individual fragments in the σ orbital. To this end, the d-electron configurations of **1–3** are best represented as $(d^8)d^1$–$d^1(d^8)$, $(d^8)d^1$–$d^1(d^6)$, and $(d^6)d^1$–$d^1(d^6)$, respectively.

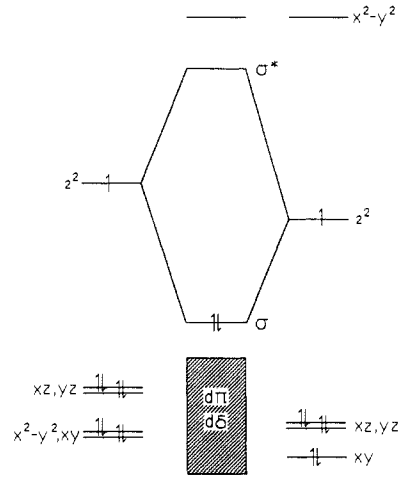

Figure 10. Qualitative level diagram for the interaction between C_{3v} Rh^0P_4 and C_{4v} $Rh^{II}P_3Cl_2$ fragments. The dπ- and dδ-symmetry orbitals are filled and indicated by the shaded box. To minimize level congestion, the σ–σ* splitting is shown to be small and the σ manifold is isolated from that of the dπ and dδ orbitals. Low-symmetry splitting within the dπ level of the C_{4v} $Rh^{II}P_3Cl_2$ fragment is not considered; interactions of the dσ and dσ* levels with the Lσ and Lσ* orbitals are also not considered.

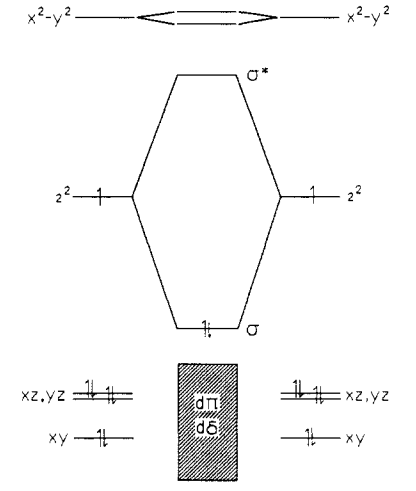

Figure 11. Qualitative level diagram for the interaction of two C_{4v} $Rh^{II}P_3Cl_2$ fragments. The dπ- and dδ-symmetry orbitals are filled and indicated by the shaded box. The σ–σ* splitting is shown to be small. Low-symmetry splittings within the dπ levels of the C_{4v} $Rh^{II}P_3Cl_2$ fragments are not considered; interactions of the dσ and dσ* levels with the Lσ and Lσ* orbitals are also not considered.

Within this framework, we see that **1** and **3** are isoelectronic with the M–M prototypes $Co_2(CO)_8$[62] and $Mn_2(CO)_{10}$,[63] respectively, and the existence of **2** formally completes the Rh–Rh single-bonded series.

On the basis of this molecular orbital model, our observation of lowest energy excited states derived from the Rh–Rh core is not surprising. The lowest energy allowed transitions are predicted to be $d\sigma \rightarrow d\sigma^*$ and $d\pi^* \rightarrow d\sigma^*$, and for **2** and **3** $\sigma(Cl) \rightarrow d\sigma^*$. Although the dσ manifold is purposely isolated from the levels of π and δ symmetries to minimize congestion in Figures 9–11, absorption spectra of the Rh_2 complexes clearly suggests a σ splitting of considerable magnitude such that the lowest energy allowed transition in **1–3** is $d\pi^* \rightarrow d\sigma^*$. In accordance with these considerations, our observation of emission from $^3(d\pi^* \rightarrow d\sigma^*)$ states follows directly from the level diagrams illustrated in Figures 9–11. Thus the similarity of the electronic absorption and emission properties of the seemingly disparate Rh_2 complexes is easily

(59) Shin, Y.-G. K.; Miskowski, V. M.; Nocera, D. G. *Inorg. Chem.*, in press.
(60) Albright, T. A.; Burdett, J. K.; Whangbo, M.-H. *Orbital Interactions in Chemistry*; Wiley-Interscience: New York, 1985; Chapters 15–19.
(61) Geoffroy, G. L.; Wrighton, M. S. *Organometallic Photochemistry*; Academic Press: New York, 1979.
(62) Abrahamson, H. B.; Frazier, C. C.; Ginley, D. S.; Gray, H. B.; Lilienthal, J.; Tyler, D. R.; Wrighton, M. S. *Inorg. Chem.* **1977**, *16*, 1554–1556.
(63) Levenson, R. A.; Gray, H. B. *J. Am. Chem. Soc.* **1975**, *97*, 6042–6047.

understood by the electronic structure models described by Figures 9-11.

The homologous series presented herein provides a basis for the synthetic design of luminescent multielectron congeners. With the two-electron mixed-valence $Rh_2(0,II)$ complex as a benchmark, the preparation of its multielectron $Rh_2(0,0)$ and $Rh_2(II,II)$ counterparts can be achieved such that a long-lived emissive $d\sigma^*$ excited state can be preserved. As is explicitly shown in Figures 9 and 10, conversion of the octahedral Rh(II) center of **2** to the trigonal-bipyramidal Rh(0) center of **1** stabilizes a formally highly energetic level that can accommodate the addition of two electrons to the metal core. In this manner, the overall electronic structure necessary for $d\sigma^*$ luminescence is preserved. Furthermore, two-electron oxidation of the Rh(0) center of **2** does not significantly perturb the σ framework because the formation of an octahedral coordination geometry destabilizes the formally occupied $d\delta$ orbital. This strategy should be completely general for several M-M systems contingent upon the successful preparation of the appropriate mixed-valence intermediate. We believe that the torsional flexibility and the electronic properties of the bis(difluorophosphino)alkylamine ligand are crucial to our success in isolating the unusual Rh_2 mixed-valence dimer, and accordingly we are continuing our efforts to assess the capacity of this ligand in stabilizing multielectron mixed-valence forms of other polynuclear metal cores. Because the Rh_2 system offers a foundation for the rational design for four-electron photocatalytic schemes, we are also extending our studies to include the possibility of photochemically interconverting between the $Rh_2(0,0)$, $Rh_2(0,II)$, and $Rh_2(II,II)$ cores.

Acknowledgment. This work was supported by the donors of the Petroleum Research Fund, administered by the American Chemical Society, and the National Science Foundation (Grant CHE-8705871). X-ray equipment was supported by a grant from the National Science Foundation (Grant CHE-8403823). D.G.N. also gratefully acknowledges a Presidential Young Investigator Award, administered by the National Science Foundation.

Supplementary Material Available: Complete tables of atomic coordinates, bond distances and angles, anisotropic temperature factors, least-squares planes, and torsional angles for **1** and **3** (26 pages); tables of observed and calculated structure factors for **1** and **3** (79 pages). Ordering information is given on any current masthead page.

Suicide Inactivation of Cytochrome P-450 Model Compounds by Terminal Olefins. 1. A Mechanistic Study of Heme N-Alkylation and Epoxidation

James P. Collman,* Philip D. Hampton, and John I. Brauman

Contribution from the Department of Chemistry, Stanford University, Stanford, California 94305-5080. *Received August 11, 1989*

Abstract: Synthetic iron porphyrins are found to be useful models for the suicide inactivation of cytochrome P-450. The epoxidation of 1-alkenes, 1,1-disubstituted alkenes, and styrenes by *meso*-[tetrakis(2,6-dichlorophenyl)porphinatoiron(III) chloride [Fe(OCP)Cl] results in the irreversible formation of *N*-alkylhemins and diminished catalytic activity. The rate of epoxide formation and the rate of N-alkylation are both first order in Fe(OCP)Cl. The efficiency of the inactivation, the number of turnovers of the catalyst per N-alkylation event, i.e., the partition number, can be measured by the ratio of epoxidation and N-alkylation rate constants. Partition numbers are found to be highly sensitive to the structure of the alkenes, somewhat sensitive to the nature of the oxygen atom donor, and relatively insensitive to the nature of the solvent. The conclusions of this study provide insight into the mechanism of the suicide inactivation of P-450 by 1-alkenes.

A wide variety of drugs and xenobiotic agents are known to destroy cytochrome P-450 activity and lead to the accumulation of green pigments in the livers of test animals.[1] Since the family of enzymes called the cytochrome P-450's are important in the degradation of xenobiotics and in the biosynthesis of steroids, the mechanism of their inactivation has been an area of extensive research. Through the work of de Matteis and Ortiz de Montellano and their co-workers, the green pigments were found to be *N*-alkylporphyrins in which a pyrrolic nitrogen of the protoporphyrin IX prosthetic group is covalently modified during substrate metabolism.[2,3]

The many oxidative transformations performed by P-450 on substrates can be classified into four main types: alkane and arene hydroxylation, heteroatom oxidation, dealkylation of heteroatoms, and olefin epoxidation.[4] These heme-containing enzymes bind a dioxygen molecule and convert it into a powerful oxidizing agent, formally an iron(V)-oxo, and release the other oxygen atom as water. Studies of a similar oxidized intermediate (HRP-I) in the enzyme horseradish peroxidase suggest the active oxidant in P-450 may more accurately be described as an oxoiron(IV) porphyrin radical cation, where the porphyrin bears one of the oxidizing equivalents.[5a] Oxygen atom donor molecules like iodosylbenzenes, hydroperoxides, and periodate can directly convert the iron(III) hemin resting state of P-450 to what is believed to be the same iron-oxo intermediate. Model studies with synthetic hemins support the above formulation of the active oxidant.[5b]

Substrate oxidation generally regenerates the iron(III) resting state of the enzyme for another cycle; however, some substrates

(1) (a) *Cytochrome P-450. Structure, Mechanism, and Biochemistry*; Ortiz de Montellano, P. R., Ed.; Plenum Press: New York, 1986; Chapter 8, pp 273-314. (b) Lavallee, D. K. *The Chemistry and Biochemistry of N-Substituted Porphyrins*; VCH Publishers: New York, 1987; Chapter 7, pp 181-207, 209-260.

(2) De Matteis, F.; Cantoni, L. *Biochem. J.* **1979**, *183*, 99.

(3) (a) Ortiz de Montellano, P. R.; Beilan, H. S.; Kunze, K. L. *J. Biol. Chem.* **1981**, *256*, 6708. (b) Ortiz de Montellano, P. R.; Yost, G. S.; Mico, B. A.; Dinizo, S. E.; Correia, M. A.; Kumbara, H. *Arch. Biochem. Biophys.* **1979**, *197*, 524. (c) Ortiz de Montellano, P. R.; Beilan, H. S.; Kunze, K. L.; Mico, B. A. *J. Biol. Chem.* **1981**, *256*, 4395. (d) Ortiz de Montellano, P. R.; Mangold, B. L. K.; Wheeler, C.; Kunze, K. L.; Reich, N. O. *J. Biol. Chem.* **1983**, *258*, 4208.

(4) Guengerich, F. P.; Macdonald, T. L. *Acc. Chem. Res.* **1984**, *17*, 9.

(5) (a) Reference 1a, Chapter 7, pp 217-271. (b) Penner-Hahn, J. E.; McMurry, T. J.; Renner, M.; Latos-Grazynsky, L.; Eble, K. S.; Davis, I. M.; Balch, A. L.; Groves, J. T.; Dawson, J. H.; Hodgson, K. O. *J. Biol. Chem.* **1983**, *258*, 12761.

0002-7863/90/1512-2977$02.50/0